

## Novel Bragg peak characterization method using proton flux measurements on plastic scintillators

Guerreiro, D. R.; Saraiva, J. G.; Peralta, L.; Rodrigues, C.; Rovituso, M.; van der Wal, E.; Schaart, Dennis R.; Crespo, P.; Simões, H.; Sampaio, J. M.

**DOI**

[10.1088/1361-6560/ad8da0](https://doi.org/10.1088/1361-6560/ad8da0)

**Publication date**

2024

**Document Version**

Final published version

**Published in**

Physics in Medicine and Biology

**Citation (APA)**

Guerreiro, D. R., Saraiva, J. G., Peralta, L., Rodrigues, C., Rovituso, M., van der Wal, E., Schaart, D. R., Crespo, P., Simões, H., & Sampaio, J. M. (2024). Novel Bragg peak characterization method using proton flux measurements on plastic scintillators. *Physics in Medicine and Biology*, 69(22), Article 225005. <https://doi.org/10.1088/1361-6560/ad8da0>

**Important note**

To cite this publication, please use the final published version (if applicable). Please check the document version above.

**Copyright**

Other than for strictly personal use, it is not permitted to download, forward or distribute the text or part of it, without the consent of the author(s) and/or copyright holder(s), unless the work is under an open content license such as Creative Commons.

**Takedown policy**

Please contact us and provide details if you believe this document breaches copyrights. We will remove access to the work immediately and investigate your claim.

***Green Open Access added to TU Delft Institutional Repository***

***'You share, we take care!' - Taverne project***

**<https://www.openaccess.nl/en/you-share-we-take-care>**

Otherwise as indicated in the copyright section: the publisher is the copyright holder of this work and the author uses the Dutch legislation to make this work public.



## PAPER

## Novel Bragg peak characterization method using proton flux measurements on plastic scintillators

RECEIVED  
5 August 2024REVISED  
25 September 2024ACCEPTED FOR PUBLICATION  
31 October 2024PUBLISHED  
11 November 2024D R Guerreiro<sup>1,2,\*</sup> , J G Saraiva<sup>1</sup> , L Peralta<sup>1,2</sup> , C Rodrigues<sup>1,2,3</sup>, M Rovituso<sup>4</sup>, E van der Wal<sup>4</sup>, Dennis R Schaart<sup>4,5</sup> , P Crespo<sup>1</sup>, H Simões<sup>1</sup> and J M Sampaio<sup>1,2</sup><sup>1</sup> Laboratório de Instrumentação e Física Experimental de Partículas (LIP), Rua Larga, 3004-516 Coimbra, Portugal<sup>2</sup> Faculdade de Ciências da Universidade de Lisboa (FCUL), Rua Ernesto de Vasconcelos, Edifício C8, 1749-016 Lisboa, Portugal<sup>3</sup> Centro de Ciências e Tecnologias Nucleares Estrada Nacional 10, ao km 139, 7, 2695-066 Bobadela, Portugal<sup>4</sup> Holland Proton Therapy Centre (HPTC), Huismansingel 4, 2629 JH Delft, The Netherlands<sup>5</sup> Department of Radiation Science and Technology, Delft University of Technology, Delft, The Netherlands

\* Author to whom any correspondence should be addressed.

E-mail: [dguerreiro@lip.pt](mailto:dguerreiro@lip.pt)**Keywords:** plastic scintillating optical fibres, Bragg peak, quality assurance, proton therapy**Abstract**

**Objective.** Bragg peak measurements play a key role in the beam quality assurance in proton therapy. Used as base data for the treatment planning softwares, the accuracy of the data is crucial when defining the range of the protons in the patient. **Approach.** In this paper a protocol to reconstruct a Pristine Bragg Peak exploring the direct correlation between the particle flux and the dose deposited by particles is presented. Proton flux measurements at the HollandPTC and FLUKA Monte Carlo simulations are used for this purpose. This new protocol is applicable to plastic scintillator detectors developed for Quality Assurance applications. In order to obtain the Bragg curve using a plastic fiber detector, a PMMA phantom with a decoupled and moveable stepper was designed. The step phantom allows to change the depth of material in front of the fiber detector during irradiations. The Pristine Bragg Peak reconstruction protocol uses the measured flux of particles at each position and multiplies it by the average dose obtained from the Monte Carlo simulation at each position. **Main results.** The results show that with this protocol it is possible to reconstruct the Bragg Peak with an accuracy of about 470  $\mu\text{m}$ , which is in accordance with the tolerances set by the AAPM. **Significance.** It has the advantage to be able to overcome the quenching problem of scintillators in the high ionization density region of the Bragg peak.

**1. Introduction****1.1. Proton therapy quality assurance**

The effectiveness of proton therapy (PT) in providing superior dose distributions to tumors and organs at risk (OARs) is well-established (De Napoli 2022, Mohan 2022, Lane *et al* 2023). Indeed, because of the Bragg Peak, PT, offers advantages over conventional x-ray-based radiotherapy, including the elimination of exit dose and the reduction in proximal dose (Mohan 2022). These benefits enable PT to minimize dose to surrounding OARs while increasing the dose to tumors, potentially lowering toxicities and enhancing the probability of local tumor control. PT is particularly appealing for head-and-neck cancers and pediatric cancer patients (Zientara *et al* 2022). Over the last decade, advances in scanning-beam technology have further improved PT, allowing intensity-modulated PT. This progress has led to a rapid growth in the number of PT centers globally, with over two hundred thousand cancer patients treated and more than one hundred operational PT facilities worldwide (Hyer *et al* 2021).

With the increasing popularity and accessibility of PT for cancer treatment, it becomes crucial to establish comprehensive Quality Assurance (QA) guidelines and methodologies. These guidelines are essential to ensure safe and effective treatment of patients, emphasizing the need for rigorous protocols in the dose delivery in PT (Mazal *et al* 1996, Arjomandy *et al* 2019).

To ensure that particle accelerator's output is consistent through time, and to ensure that beam parameters used for treatment planning remain exact, regular machine QA procedures (Arjomandy *et al* 2009) are necessary. Dosimetry parameter checks, represent one part of the Delivery Techniques category, involving the monitoring of absolute absorbed dose to the target and relative dose distributions (Arjomandy *et al* 2019). The Bragg Peak is the primary factor that distinguishes PT from conventional radiotherapy methods, so these QA procedures focus on the study of the BP's longitudinal and transversal profile. For instance, in a pencil beam scan as used in this study (Arjomandy *et al* 2019) the pertinent parameters are:

longitudinal profile

- The range in water of the pristine Bragg Peak, defined as the position of the distal 90% dose value.
- The distal dose falloff (that is used to analyse the energy spread of the beam) defined as the distance between the positions of the distal 80% and 20% value of dose.

transversal profile

- The centroid position.
- The full width at half maximum or one sigma of its Gaussian representation, measured at a specific position and the shape of the beam spot.

For dosimetric measurements the gold standard is the ionization chamber (IC). In the case of PT, the most suitable is the Markus IC (Pearce *et al* 2006, Arjomandy *et al* 2008). ICs present high sensitivity, wide dynamical range, stability and a predicable response. The disadvantages of the IC include their bulkiness that results in a spatial resolution that is not at the same level as other detectors. Also, ICs present temperature and pressure dependence. Recombination losses in the sensitive air volume limits their application in emerging techniques, such as FLASH radiotherapy (Siddique *et al* 2023).

Diode detectors are another option when it comes to the Bragg Peak profile measurements. These detectors are gaining popularity due to their small size that translates into good spatial resolution (hundreds of  $\mu\text{m}$ ). Measurements suggest that diode response dependence on linear energy transfer (LET) is negligible for low-LET proton (Schönfeld *et al* 2019). Fast response times, as low as several ns, have been reported (De Napoli 2022).

Scintillators are also used for proton QA measurements, as is the case of this study. Plastic scintillators exhibit high sensitivity to ionizing radiation, making them effective detectors for various applications, including medical dosimetry and radiation monitoring (Lee *et al* 2019). They have fast response time ( $\approx 10$  ns), providing quick and real-time measurements of dose distribution (Lyons and Stevens 1974). Being low atomic number ( $Z$ ) materials, plastic scintillators are relatively tissue-equivalent, making them interesting for dosimetry in medical applications where equivalent tissue response is desirable (Kim *et al* 2016).

## 1.2. Plastic scintillator's quenching

Birks' law, describes the non-linear relationship between the scintillation light yield and the energy deposition of ionizing radiation in organic scintillating materials (Birks 1951). Stated by physicist John B Birks in the 1950s, the law describes a reduction in scintillation light output at high ionization densities, known as the quenching effect. This effect is prominent at high-LET or at high-energy deposition rates. The law is formulated as:

$$\frac{dL}{dx} = \frac{S \cdot \frac{dE}{dx}}{1 + k_B \cdot \frac{dE}{dx}}, \quad (1)$$

where  $\frac{dL}{dx}$  is the scintillation light output per unit path length,  $\frac{dE}{dx}$  is the stopping power,  $S$  the scintillation efficiency at zero ionization density, and  $k_B$  the Birks constant. This constant is material-specific, representing the susceptibility of a scintillator to quenching and can be experimentally determined. Understanding Birks' quenching is crucial in designing and calibrating scintillation detectors, especially in situations involving high ionization density or varying radiation types. The deviation from linearity can, however, be mitigated by employing compensation techniques reducing quenching effects and ensuring accurate detector responses. Although the Birks' formula is considered the best approach to model a scintillator's quenching it is important to mention that among its limitations is the fact that it fails when it comes to mixed particle fields. This happens because the track structure varies with particle energy and particle type. For example, it is possible to have different  $k_B$  factors for protons and helium ions even if they have the same LET because they exhibit different track structures (Christensen *et al* 2019).

Correcting for Birks' quenching is the object of previous works: the determination of a relationship between the particle's LET and the quenching correction factor was studied in Wang *et al* (2012) achieving an

agreement of 5% with the ionization chamber. Corrections performed using analytical LET values resulted in doses within 1% of those obtained using Monte Carlo LET values in Robertson *et al* (2013). The doping of optical fibres with gadolinium was studied in Penner *et al* (2018) to make the fibres response less quenching dependent. The usage of fluorescence light instead of scintillation light has also been explored as a way to avoid the quenching problem in plastic optical fibres (Christensen *et al* 2018). As mentioned before, scintillators present fast signals and their usage for timing applications is well documented, presenting signal duration that ranges from 0.35 to 10 ns. This characteristic of the organic scintillators is of upmost importance in this study where is proposed the usage of scintillators to measure the flux of protons at certain depths and the employment of this information for the reconstruction of the Bragg Peak.

## 2. Methods

### 2.1. Detector and phantom setup

The sensitive region of the detector is constituted by 64 Scintillating Plastic Optical Fibre (SPOF) of 1 mm in diameter (Kuraray SCSF-78) aligned and juxtaposed as an array (figure 1) (Guerreiro *et al* 2024). The fibre's signal is read by a H8500C Multi-Anode PhotoMultiplier (MAPMT) placed on the top end of the fibres. In the beam tests only the 16 central fibres are directly exposed, as only 16 electronic channels were available.

To measure the proton beam profile, a PMMA step phantom was built as shown in figure 2(a). The phantom has 15 steps starting from a minimum thickness of 19.7 mm up to maximum thickness of 26.7 mm, in 0.5 mm increments. Each step is 18 mm wide to match the 1 mm × 16 fibres. Extra 2 mm were added to ensure a tolerance in the positioning of the phantom in front of the optical fibres. During irradiation the phantom moves in front of the detector with the help of a stepper motor, as can be seen in figure 2(b).

The phantom includes a fixed part composed by a 59 mm thick PMMA slab to reach the Bragg peak conditions. This way, the proton beam has to traverse the step phantom and the fixed part of the phantom. So, the maximum reachable thickness is equal to 110.7 mm (including movable, fixed part of the phantom and an 25 mm of PMMA used for higher energies). This slab is fixated inside the detector and is designed in such a way as to block room light and to ensure there are no air gaps between itself and the optical fibres (a CAD model can be seen in figure 3). A second slab is placed on the opposite side of the detector to ensure that there is material continuity after the optical fibres and to account for the backscattering of protons and secondary particles.

A light tight box embeds the phantom PMMA bulk, the fiber array and the MAPMT avoiding contamination from external light sources, (see figure 3). The noise measured prior to the experiments was  $47 \pm 6$  Hz, this results in a Signal-to-Noise ratio of about 1000 in these set of measurements. Moreover, the irradiation box serves to ensure the connection between the SPOFs and the MAPMT is mechanically stable and the positioning of the phantom relative to the SPOFs is reproducible. A printed circuit board placed on top of this irradiation box is designed to make the interface between the MAPMT and the DAQ through 2 meter long coaxial cables with LEMO FGG.0B.304.CLAD52Z connectors.

### 2.2. Electronic readout

The available electronic setup enabled the readout of 16 MAPMT channels, connected to NIM discriminators (Phillips Scientific Octal Discriminator NIM MODEL 705). These discriminators were set at a threshold of  $-100$  mV and have an output signal of 1 V. This signal is read by a NIM-ECL translator and then transmitted to a ECL-differential translator. The differential signal is read by the TRB3 board.

The TRB3 is a multipurpose 1 + 4 FPGA board that was developed at GSI for the HADES experiment (Neiser 2013). It has a FPGA-based 64 + 1 channel Time-to-Digital (TDC) converter. TDC is a circuit used to timestamp events and measure time differences between events, especially where high accuracy is required (Kalisz 2003). The used TDCs have a time precision down to 3.6 ps and can get up to 50 MHz signal rates (burst). The TRB3 software allows the measurements of signal rates, through the usage of an signal counter at increments up to a total of 20 G signals before resetting. The signal rate can be determined by reading the signal counter at fixed time intervals and dividing the it by the time interval width in seconds.

The TRB3 communicates with a OIROID single-board computer and the users laptop through a local network. The readout diagram can be seen in figure 4. This setup allows the user's personal computer to communicate with the inside of the bunker.

The readout chain's accuracy was checked using a signal generator, set to emulate a PMT signal. The readout as a function of the signal's frequency can be seen in figure 5. The tests showed that there is a systematic deviation of the system readout of 7.5%. This is taken into account when calculating the error in the measurements.

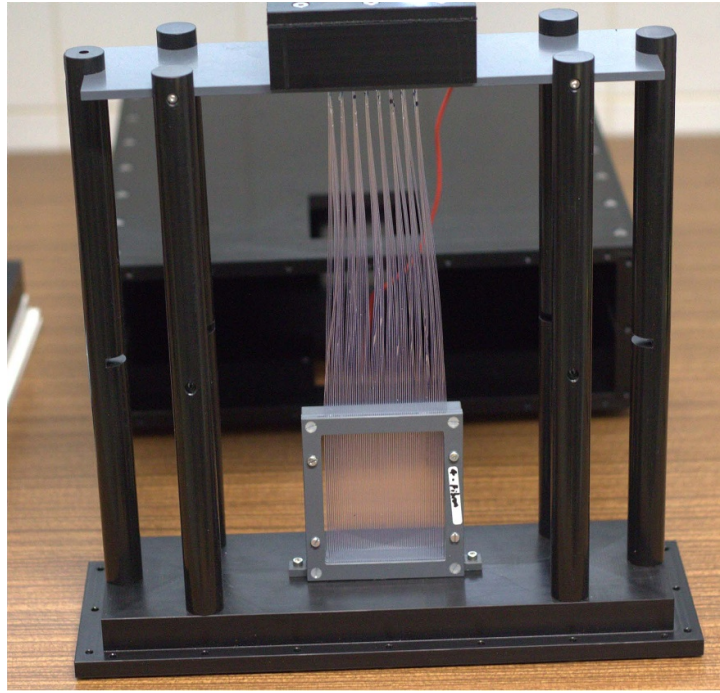
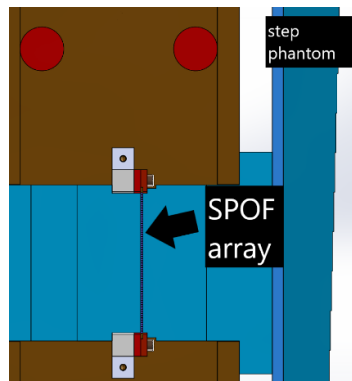
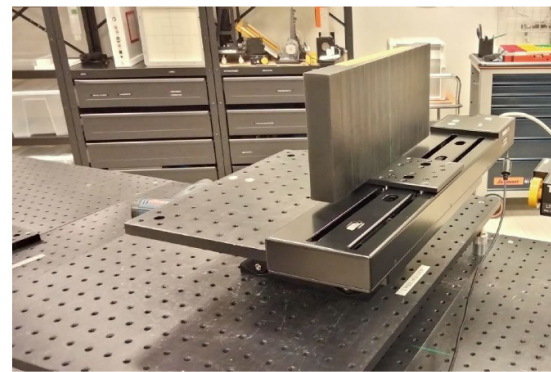


**Figure 1.** Inside of the detector. The arrays are comprised of 64 SPOFs although during the irradiations only the 16 central fibres were used.



(a)



(b)

**Figure 2.** (a) Top view of part of the detector and the PMMA step phantom used during irradiation. On the left hand side of the phantom it is possible to see the 0.5 mm increments. (b) Phantom placed on the stepper table. The phantom slides horizontally to position a different PMMA thickness in front of the 16 active fibres.

### 2.3. HollandPTC R&D beamline

The experimental room of HollandPTC (Delft, Netherlands) is equipped with a fixed horizontal proton beam line. The beam is produced by a Varian ProBeam isochronous cyclotron which can deliver a therapeutic proton beam of energies between 70 and 240 MeV with beam currents between 1 nA and 800 nA at cyclotron extraction. The current was chosen taking into account the TRB3's bandwidth of  $30 \times 10^7$  signals/second and the beam characterization done at HollandPTC (Groenendijk *et al* 2023). For these measurements, a pencil beam configuration was used with 130 MeV energy and 1 pA current at target. At this energy the beam width was  $\sigma = 4.19$  mm. The detector was aligned using the in-house alignment system at HollandPTC.

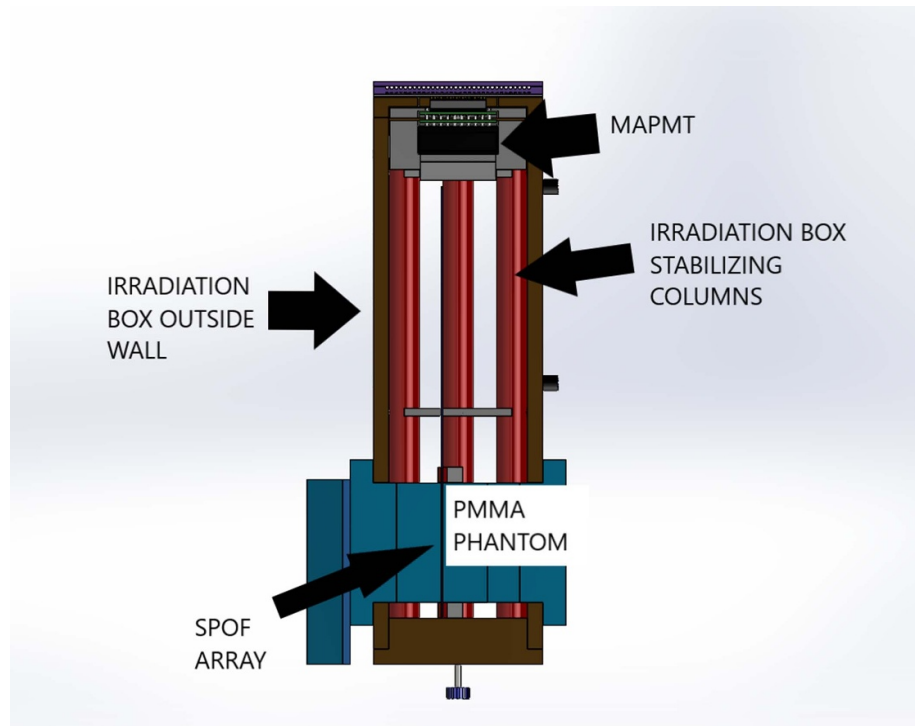


**Figure 3.** CAD model of the detector and phantom setup. A view was selected to highlight that the phantom (blue) fills the detector in such a way that it eliminates the air gaps and the guarantees the continuity of material before and after the optical fibres.

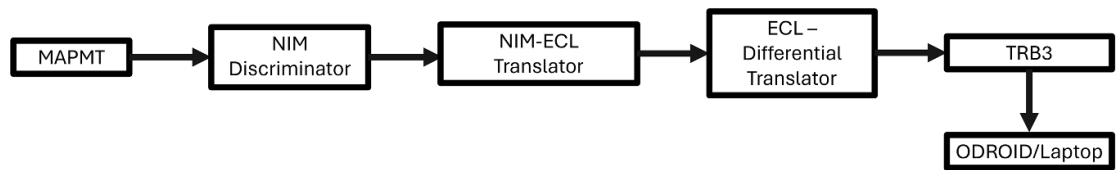


**Figure 4.** Readout chain block diagram.

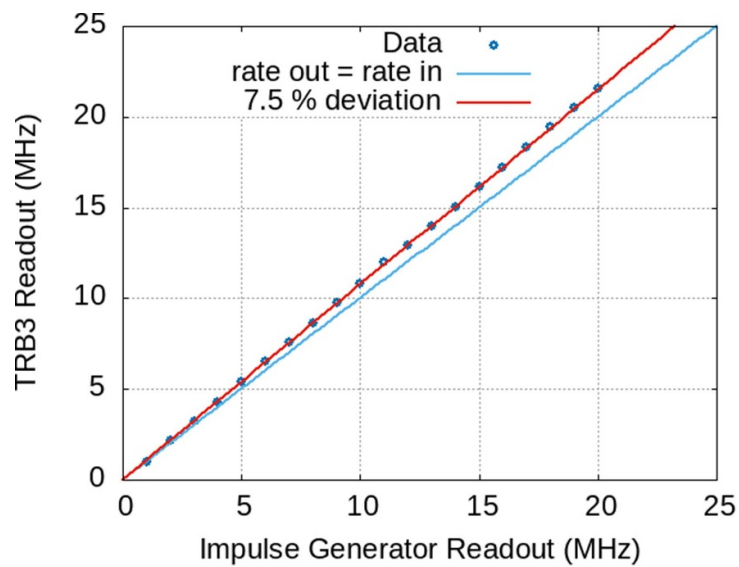
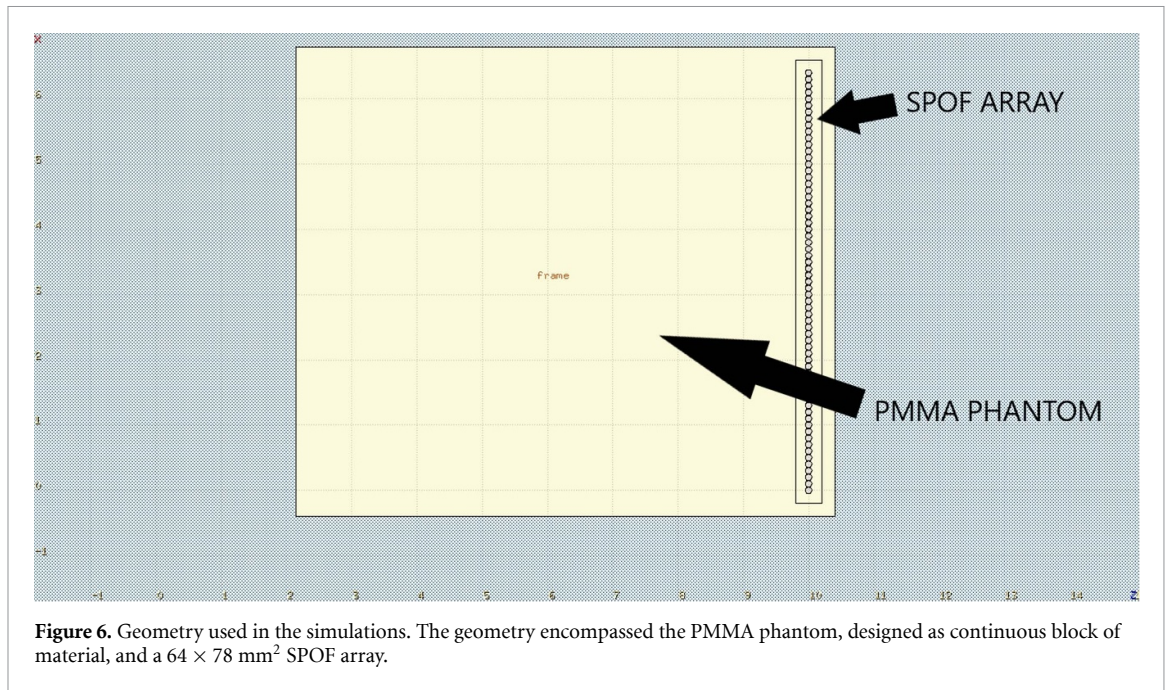


**Figure 5.** TRB3 readout has a function of the input signal's frequency. The line represents the TRB3 output rate equal to the generator input rate.



#### 2.4. The Bragg peak reconstruction method

The method for the reconstruction of the Bragg curve from experimental particle-SPOF interaction rate measurements is as follows. The dose at each position is obtained from the product of the particle—SPOF interaction rate by the average particle dose according to the equation

$$D(z) = hr_{\text{data}}(z) \times \left[ \frac{D_{\text{Total}}(z)}{hr(z)} \right]_{\text{MC}}, \quad (2)$$

where  $D(z)$  is the dose deposited at each depth of PMMA,  $hr_{\text{data}}(z)$  is the measured particle-SPOF interaction rate at each depth, and  $\left[ \frac{D_{\text{Total}}(z)}{hr(z)} \right]_{\text{MC}}$  is the total dose at each depth divided by the number of particles that reach the SPOFs, calculated using FLUKA 4-3.4 (Vlachoudis 2009, Battistoni 2015, Ahdida 2022).

In these simulations, the geometry encompassed the PMMA phantom, designed as continuous block of material, and a SPOF array. The SPOFs used in the simulations resemble the ones available for the assembly of the detector. They have a cladding made of Poly(methyl methacrylate) (PMMA) and a core made of polystyrene. The SPOFs are cylindrical in shape with 1 mm in diameter (97% core and 3% cladding), as can be seen in figure 6. A USRBIN scorer is used to calculate the total deposited dose, while an EVENTBIN scorer is employed to determine the number of particles interacting with the SPOFs. In both cases, the bin size is set equal to the volume of each SPOF. The data recorded in each bin is accumulated across all bins and then normalized by the number of particles reaching the bins at each depth. Consequently, the mean deposited dose is calculated by dividing the total dose recorded by USRBIN by the number of particles entering the SPOFs, as determined by EVENTBIN. This result is illustrated in figure 7.

### 3. Results and discussion

For each one of the 16 fibres the TRB3 readout gives the number of proton-SPOF interactions per unit of time. This value is correlated to the proton flux at each depth of PMMA reaching that fiber. For the data acquisition in each depth several proton beam shots were performed. The detector's response precision can be analysed through each SPOF's response at each position. The individual response for each SPOF can be seen in figure 8. For each position the set of fibres irradiated exhibit a dispersion between 1% and 4%.

To obtain the experimental particle-SPOF interaction rate, and in order to avoid loss of information due to the pencil beam's dispersion, the 16 SPOF signals were summed. A comparison between the simulated and the measured particle-SPOF interaction rate is presented in figure 9, both normalized to the first position.

From figure 9, we get that the measured proton-SPOF interaction rate is within 15% of the simulated proton-SPOF interaction rate. It is also noticeable that the experimental data is below the simulated data for

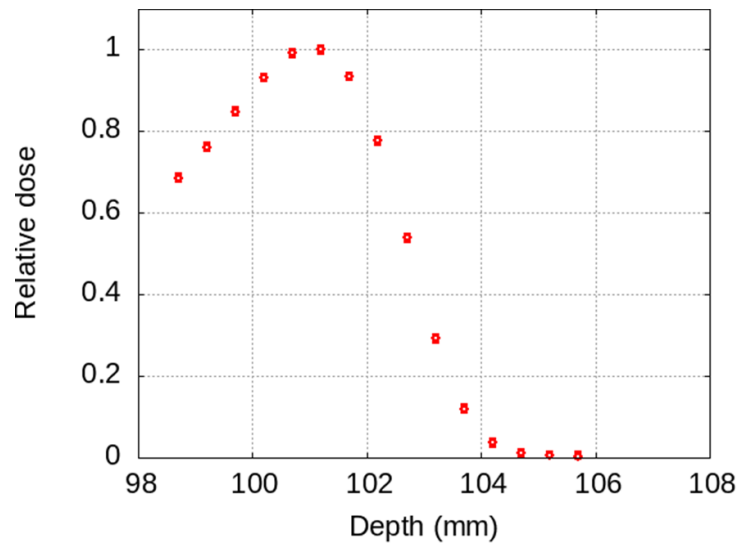


Figure 7. Relative dose deposition for each simulated depth.

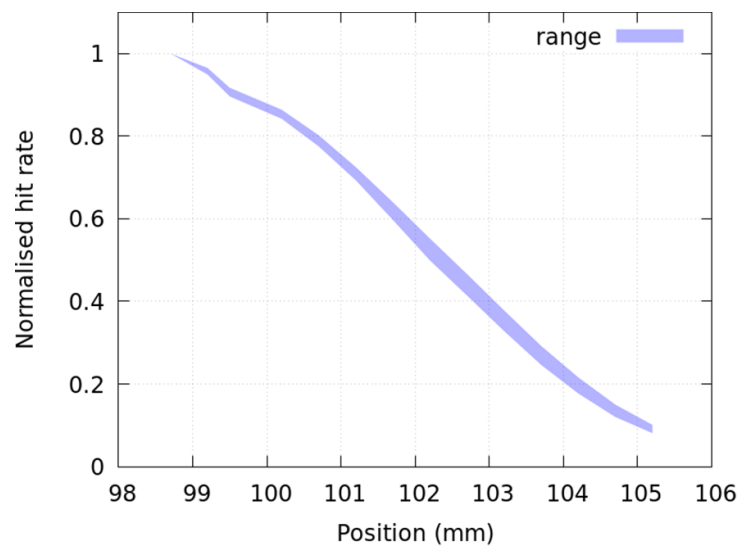


Figure 8. Normalised particle-SPOF interaction rate for each fiber and step position. The normalisation is made dividing each fibre response by its mean response value over all thickness used.

depths above 104,7 mm. This behaviour is explained considering that the particles that reach the SPOF's beyond that point may not create a scintillation signal with enough amplitude to go over the NIM discriminator threshold.

The result of the reconstruction of the Bragg Peak is presented in figure 10(a), and the residuals for every point can be seen in figure 10(b).

The positions obtained experimentally and simulated for the maximum dose percentages that the AAPM recommends in their QA protocol (Arjomandy *et al* 2009) are presented in table 1.

Comparing the depth values for each reference dose level a difference of  $\leq 470 \mu\text{m}$  between the experimental and simulated positions obtained. These discrepancies between positions are within the requirements set by the AAPM, given that they set a 1 mm maximum resolution for QA measurements (Arjomandy 2019). The uncertainty in the experimental points is given by the uncertainty of the phantom step thickness. The uncertainty of the Monte Carlo data is given by the bin size used in the simulation.

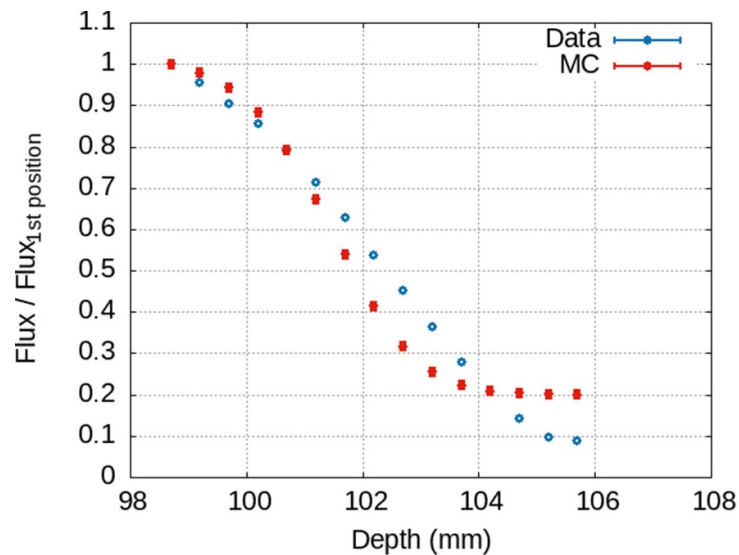


**Figure 9.** Comparison between the simulated proton flux and the measured proton-SPOF interaction rate after the sum of the 16 channels. Error bars too small to be seen.

#### 4. Conclusion

In this study a first proof-of-concept for using a SPOF array for QA in PT was presented. First tests with a proton beam were carried on at the HollandPTC R&D beamline using a pencil beam with a single energy of 130 MeV. Future analysis should cover the 70–250 MeV range to validate this technique.

A new methodology, combining MC simulations and proton-SPOF interaction rate measurements was developed, allowing to circumvent the LET dependence of the signal produced in the SPOFs. This methodology differs from other methods, cited in this paper, because it does not look to use the Birk's model to correct the scintillator's signal amplitude. Instead of measuring the signal's amplitude, this technique focuses on the measurement of the particle-SPOF interaction rate in a certain position. This technique, although CPU time-consuming and dependent on prior knowledge of the irradiation setup, is well adapted to beam quality control. The knowledge of beam energy is a key component of the method, although not necessarily a handicap. In the present tests, 16 electronic channels were available, but the employment of a higher number of electronic channels would allow the scan of the transverse beam profile. This is also a very important quantity when it comes to the QA activities defined by the AAPM.

The experimental measurements have shown that the detector presents a standard deviation below 4% across all the SPOFs read. The comparison between the proton-SPOF interaction rate measured and simulated has shown a deviation below 15%. The combination of this experimental proton-SPOF interaction rate and the mean deposited dose taken from FLUKA simulation has shown to be able to reconstruct the Bragg Peak with an accuracy  $\leq 470 \mu\text{m}$ .

Several techniques could be implemented to improve the presented method, like the usage of faster scintillators, that trade the signal's amplitude accuracy for a faster signal (García Díez *et al* 2023). A faster signal would improve the timing resolution of the scintillator, avoiding signal pileup. The usage of an electronic board with a larger bandwidth would allow the monitoring of higher intensity beams.

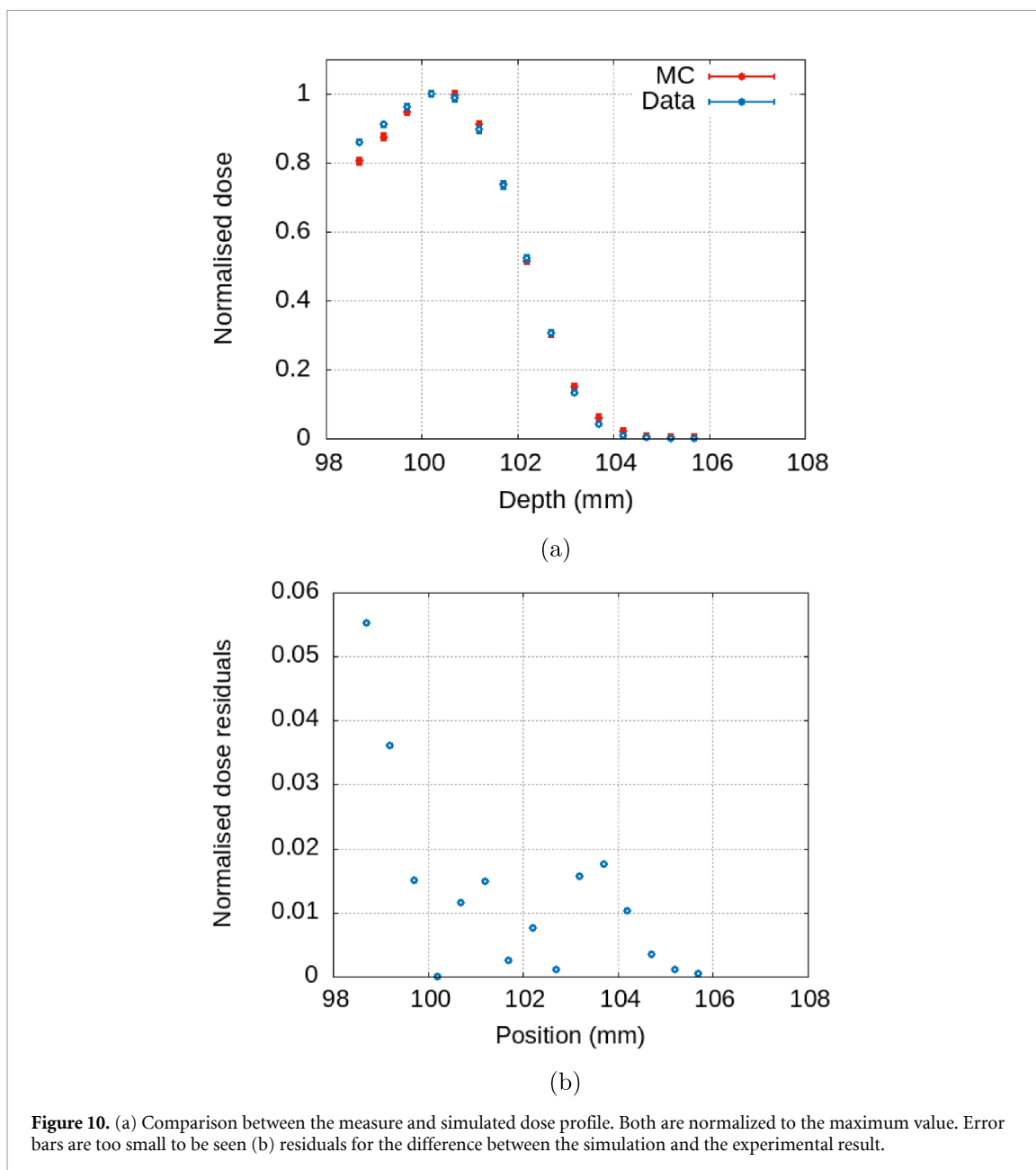


**Figure 10.** (a) Comparison between the measure and simulated dose profile. Both are normalized to the maximum value. Error bars are too small to be seen (b) residuals for the difference between the simulation and the experimental result.

**Table 1.** Longitudinal profile positions for the experimental and simulated values in mm. The distal dose fall off is calculated as the distance between distal 20% and distal 80% of the maximum. The deviations,  $\Delta$ , between the experimental measurements and the simulation are also presented.

	Proximal 90% (mm)	Distal 90% (mm)	Distal 80% (mm)	Distal 20% (mm)	Distal fall-off (mm)
Experimental	$99.09 \pm 0.08$	$101.2 \pm 0.08$	$101.49 \pm 0.08$	$103.01 \pm 0.08$	$1.75 \pm 0.11$
Monte Carlo	$98.87 \pm 0.50$	$101.2 \pm 0.50$	$101.52 \pm 0.50$	$102.53 \pm 0.50$	$1.5 \pm 0.50$
$\Delta$	$-0.2 \pm 0.50$	$+0.04 \pm 0.50$	$+0.02 \pm 0.50$	$-0.47 \pm 0.50$	$+0.25 \pm 0.51$

### Data availability statement

The data that support the findings of this study are available upon reasonable request from the authors.

## Acknowledgments

This work is partially funded by the Fundação para a Ciência e Tecnologia (FCT) Grant Reference CERN/FIS-TEC/0017/2021 (ImprovPT project). D R G is supported by the FCT Scholarship Reference SFRH/BD/150786/2020 (PT-CERN PhD Grants). C R is supported by the FCT Scholarship Reference PRT/BD/153500/2021. The authors acknowledge research center funding Reference UIDP/50007/2020 (LIP). The authors recognize LIP's mechanical workshop input to this work in the form of production of the PMMA phantom. LIP's Detector Laboratory contribution is also recognized, in the person of Alberto Blanco and João Saraiva, for allowing the usage of TRB3. The authors are indebted to the HollandPTC for the use of their facilities and provided beamtime.

## ORCID iDs

D R Guerreiro  <https://orcid.org/0000-0002-9453-6871>

J G Saraiva  <https://orcid.org/0000-0002-7006-0864>

L Peralta  <https://orcid.org/0000-0002-3834-1762>

Dennis R Schaart  <https://orcid.org/0000-0002-3199-5608>

## References

- Ahdida C *et al* 2022 New capabilities of the FLUKA multi-purpose code *Front. Phys.* **9** 788253
- Arjomandy B *et al* 2019 AAPM task group 224: comprehensive proton therapy machine quality assurance *Med. Phys.* **46** e678–705, 689
- Arjomandy B, Sahoo N, Ding X and Gillin M 2008 Use of a two-dimensional ionization chamber array for proton therapy beam quality assurance *Med. Phys.* **35** 3889–94
- Arjomandy B, Sahoo N, Zhu X R, Zullo J R, Wu R Y, Zhu M, Ding X, Martin C, Ciangaru G and Gillin M T 2009 An overview of the comprehensive proton therapy machine quality assurance procedures implemented at The University of Texas M. D. Anderson Cancer Center Proton Therapy Center–Houston *Med. Phys.* **36** 2269–82
- Arjomandy B *et al* 2019 AAPM task group 224: comprehensive proton therapy machine quality assurance *Med. Phys.* **46** e678–705
- Battistoni G *et al* 2015 Overview of the FLUKA code *Ann. Nucl. Energy* **82** 10–18
- Birks J B 1951 Scintillations from organic crystals: specific fluorescence and relative response to different radiations *Proc. Phys. Soc. A* **64** 874
- Christensen J B, Almhagen E, Nyström H and Andersen C E 2018 Quenching-free fluorescence signal from plastic-fibres in proton dosimetry: understanding the influence of Čerenkov radiation *Phys. Med. Biol.* **63** 065001
- Christensen J B, Almhagen E, Stolarczyk L, Vestergaard A, Bassler N and Andersen C E 2019 Ionization quenching in scintillators used for dosimetry of mixed particle fields *Phys. Med. Biol.* **64** 095018
- De Napoli M 2022 Sic detectors: a review on the use of silicon carbide as radiation detection material *Front. Phys.* **10** 898833
- García Díez M, Espinosa Rodríguez A, Sánchez Tembleque V, Sánchez Parcerisa D, Valladolid Onecha V, Vera Sanchez J A, Mazal A, Fraile L M and Udias J M 2023 Technical note: measurement of the bunch structure of a clinical proton beam using a SiPM coupled to a plastic scintillator with an optical fiber *Med. Phys.* **50** 3184–90
- Groenendijk C F, Rovituso M, Lathouwers D and Brown J M C 2023 A Geant4 based simulation platform of the HollandPTC R&D proton beamline for radiobiological studies *Phys. Med.* **112** 102643
- Guerreiro D R, Saraiva J G, Borges M J, Sampaio J M and Peralta L 2024 Development of a plastic scintillating optical fibers array dosimeter for radiobiology *J. Instrum.* **19** 05006
- Hyer D E, Ding X and Rong Y 2021 Proton therapy needs further technological development to fulfill the promise of becoming a superior treatment modality (compared to photon therapy) *J. Appl. Clin. Med. Phys.* **22** 4–11
- Kalisz J 2003 Review of methods for time interval measurements with picosecond resolution *Metrologia* **41** 17
- Kim Y, Yoo H, Kim C, Taek Lim K, Moon M, Kim J and Cho G 2016 Plastic scintillator for radiation dosimetry *Radiat. Prot. Dosimetry* **170** 187–90
- Lane S A, Slater J M and Yang G Y 2023 Image-guided proton therapy: a comprehensive review *Cancers* **15** 2555
- Lee U, Nyun Choi W, Woo Bae J and Reyoung Kim H 2019 Fundamental approach to development of plastic scintillator system for in situ groundwater beta monitoring *Nucl. Eng. Technol.* **51** 1828–34
- Lyons P B and Stevens J 1974 Time response of plastic scintillators *Nucl. Instrum. Methods Phys. Res.* **114** 313–20
- Mazal A, Habrand J L, Lafortune F and Breteau N 1996 Quality assurance in protontherapy: a systematic approach in progress at Orsay *Bull. Cancer Radiother.* **83** 179s–84s
- Mohan R 2022 A review of proton therapy—current status and future directions *Precis. Radiat. Oncol.* **6** 164–76
- Neiser A *et al* 2013 TRB3: a 264 channel high precision TDC platform and its applications *J. Instrum.* **8** C12043
- Pearce J, Thomas R and Dusautoy A 2006 The characterization of the Advanced Markus ionization chamber for use in reference electron dosimetry in the UK *Phys. Med. Biol.* **51** 473–83
- Penner C, Hoehr C, O'Keeffe S, Woulfe P and Duzenli C 2018 Characterization of a terbium-activated gadolinium oxysulfide plastic optical fiber sensor in photons and protons *IEEE Sens. J.* **18** 1513–9
- Robertson D, Mirkovic D, Sahoo N and Beddar S 2013 Quenching correction for volumetric scintillation dosimetry of proton beams *Phys. Med. Biol.* **58** 261–73
- Schönfeld A B, Poppinga D, Kranzer R, De Wilde R L, Willborn K, Poppe B and Looe H-K 2019 Technical note: characterization of the new microsilicon diode detector *Med. Phys.* **46** 4257–62

- Siddique S, Ruda H E and Chow J C L 2023 Flash radiotherapy and the use of radiation dosimeters *Cancers* **15** 3883
- Vlachoudis V 2009 Flair: a powerful but user friendly graphical interface for fluka *Proc. Int. Conf. on Mathematics, Computational Methods & Reactor Physics (M&C 2009) (Saratoga Springs, New York)*
- Wang L L, Perles L A, Archambault L, Sahoo N, Mirkovic D and Beddar S 2012 Determination of the quenching correction factors for plastic scintillation detectors in therapeutic high-energy proton beams *Phys. Med. Biol.* **57** 7767–81
- Zientara N, Giles E, Le H and Short M 2022 A scoping review of patient selection methods for proton therapy *J. Med. Radiat. Sci.* **69** 108–21